



## Breaking failure analysis and finite element simulation of wear-out winding hoist wire rope

Xiang-dong Chang<sup>a,b,c</sup>, Yu-xing Peng<sup>a,b,c,\*</sup>, Zhen-cai Zhu<sup>a,b</sup>, Xian-sheng Gong<sup>d</sup>,  
Zhang-fa Yu<sup>e,f,g</sup>, Zhen-tao Mi<sup>a,b</sup>, Chun-ming Xu<sup>a,b</sup>

<sup>a</sup> School of Mechanical and Electrical Engineering, China University of Mining and Technology, Jiangsu Province, Xuzhou 221116, China

<sup>b</sup> Jiangsu Key Laboratory of Mine Mechanical and Electrical Equipment, China University of Mining & Technology, Jiangsu Province, Xuzhou 221116, China

<sup>c</sup> Jiangsu Collaborative Innovation Center of Intelligent Mining Equipment, Xuzhou, China

<sup>d</sup> College of Mechanical Engineering, Chongqing University, Chongqing 400044, China

<sup>e</sup> Citic Heavy Industries Co. Ltd, Luoyang, China

<sup>f</sup> Luoyang Mining Machinery Engineering Design Institute Co. Ltd, Luoyang, China

<sup>g</sup> State Key Laboratory of Mining Heavy Equipment, CITIC HIC, Luoyang, China



### ARTICLE INFO

#### Keywords:

Wire rope  
Wear  
Breaking failure  
Finite element simulation

### ABSTRACT

Surface wear is the main reason for the breaking failure of the wire rope in service, particularly in the multi-layer winding hoist system of a coal mine. Understanding the effect of wear scars on the failure and mechanical properties of the rope is the effective way to ensure the safety of multi-layer winding hoist. In this paper, the breaking failure characteristics of hoist ropes with different wear scars were investigated by the breaking tensile test. The temperature rise in the wear scar regions was obtained and analyzed. Additionally, the finite element method was used to simulate the mechanical properties of the wear-out strands subjected to tensile load. Results show that the severe plastic deformation and obvious temperature rise occur in the wear scar region. The temperature rise curves during the breaking tensile test can reflect the number and the order of the fractured strands. The wear-out outer wires fracture earlier than the internal wires, and the wires with irregular wear scar always fracture along the sliding wear direction at the location with the maximum wear depth. Additionally, the wear scar caused by left cross contact will cause stress concentration and uneven distribution, and the wear depth makes it more obvious.

### 1. Introduction

Wire rope is a critical component of multi-layer winding hoist system because of its unique mechanical properties (high axial capability and flexibility in bending) [1,2]. It determines the mine hoist safety and hoisting capacity for the system. However, during the winding hoist, in particular for an ultra-deep coal mine, the hoisting system vibration caused by the changing vertical rope length and inertial load will result in dynamic tension of the rope at both end [3,4], which will cause severe extrusion and relative sliding between wire ropes among layers. Additionally, winding hoist wire rope always operate at high stress and almost invariable subject to fluctuating loads [5,6]. It is easy to lead to external wear and plastic deformation, the primary degradation mechanism of wire rope operating on mine hoisting drums [7], under that condition. Furthermore, as the wire rope winds on and off drums in the process of

\* Corresponding author at: School of Mechanical and Electrical Engineering, China University of Mining and Technology, Jiangsu Province, Xuzhou 221116, China.

E-mail address: [pengyuxing@cumt.edu.cn](mailto:pengyuxing@cumt.edu.cn) (Y.-x. Peng).

hoisting, this degradation will occur periodically and be accelerated, which seriously affects its mechanical properties, reduces the service life and ultimately leads to breaking failure of the rope [8]. Moreover, to reduce the effects of the wear on the safety use for wire ropes, the number of winding layers on the drum is limited to two layers according to the coal mine safety rules in China [9], which will cause the increase of the drum size for the winding equipment and hinder the development of resource exploitation in the ultra-deep coal mine. Therefore, it is of great importance to investigate the effects of the surface wear on the breaking failure behaviour and the mechanical properties for the winding hoist wire rope, which contributes to the reasonable use of the wire rope and provides the basis for the design of the multi-layer winding hoist in ultra-deep coal mines.

Several studies have been conducted on the related characteristics of the wire rope by others in the past decades. As the wear is one of the main reasons for the failure of the wire rope, Zhang et al. [10] investigated the fretting wear and fatigue mechanisms of the steel wire in hoisting rope through experiments and found that the wear mechanism depends on the contact loads. Wang et al. [11,12] researched the effects of different contact conditions on the fretting fatigue damages of the mine rope wires in different corrosive media. The results show that the fretting damage and crack nucleation accelerate with increasing displacement amplitude. Additionally, the effect of the terminal mass on the fretting parameters during a lifting cycle was also analyzed [4]. Cruzado et al. [13,14] studied the effect of contact pressure and crossing angle on the fretting wear scar and the coefficient of wear for thin steel wires. The finite element method was also used to simulate and predict the variation of the wear scars in the fretting regions [15,16]. They found that the wear occurring in the steady state period is rather mild. Furthermore, to analyze the failure behaviour of the wire rope, Chaplin et al. [5,17] analyzed the failure mechanisms of the hoisting wire rope in different applications, which is important in realising the potential rope life. Considering the specific working conditions of multi-layer winding hoist, Rebel et al. [7] discussed the influence of different winding hoist parameters on the rate of rope deterioration, which will aid in the design of winding system due to a better understanding of the key factors that influence rope performance on multi-layer drums. Mahmoud et al. [18] determined the fracture strength of a cracked suspension bridge wire based on liner elastic fracture mechanism and presented a case study for a group of in situ wire breaks retrieved from a suspension bridge cable. Singh et al. [6] carried out detailed research for the causes of failure of two wire ropes from two different Indian underground coal mines. Different damage parameters (wear & corrosion, lubrication, macro & micro-examination and chemical composition) were also investigated and found that the excessive wear and corrosion are the major causes of failure. Peterka et al. [19] researched the reason of the steel rope damage in a hoisting system. The analysis found that the upper wires of the rope with different strength grades will lead to different deformation of the wires and the development of fractures at the weaken places. Piskoty et al. [20] emphasised the importance of making a broad collection of hypotheses at the beginning of failure investigations and presented four case studies of structural failures, where the failed load carrying structure was based on wire rope (steel cables). Additionally, the experience made by a failure analysis is recallable and applicable for different kinds of failed systems. Additionally, Karabay et al. [21] investigated different wire damages and defects during different processing steps of aluminum conductor production and explained the early failure reasons. Yu et al. [22] proposed a theoretical approach and a finite element method model to calculate recovery length and the force redistribution mechanism in a semi-parallel wire cable with broken wires. They found that the twist angle and position of the broken wire will affect the recovery length.

As the safety use and service life of the wire rope are the most important things in different applications, Giglio et al. [23] established two analytical models to investigate the stress and strain of a wire rope subjected to axial and bending loads. The results are in close agreement with the experimental results obtained, which make it possible to reliably predict the fatigue life of a wire rope. To study the defective strand inside the internal structure of a multi-wire rope, Raišutis et al. [24] investigated the propagation of ultrasonic guided waves (UGW) along multi-wire ropes with polymer cores and developed an ultrasonic testing technique to identify defective strands inside the rope, which is sufficient reliability for practical. Zhao et al. [25] analyzed and calculated the fatigue life of a wire rope based on the theory of stress field intensity and linear fatigue cumulative damage theory. Then, the theoretical value was compared with the experimental value and they are close to each other in the fatigue cycle. Additionally, taking into account the complex structure of the wire rope and the high cost (time and economic) for the experimental investigation, the finite element method (FEM) was widely used to study the related characteristics of the wire rope. Lalonde et al. [26,27] proposed a FE modelling strategy for multilayered stands and used this model to study Aluminum Conductor Steel Reinforced (ACSR) subjected to wind-induced loads. The results indicate that fatigue prediction from the Coffin-Manson relation associated with the FE model provide realistic evaluations of service lives. Stanova et al. [28,29] presented the geometric models of the single-lay wire strands and double-lay wire ropes with defined initial parameters and the model was used to predict the strand's behaviour under tensile load through a finite element program. Then, mechanical behaviour of the spiral triangular strands and oval strands under axial loads were also analyzed [30,31]. Wang et al. [32,33] explored the fretting fatigue parameters and stress distributions of the hoisting rope and three-layered strand using the finite element method. They established the relationship between the crack propagation life of steel wire and the initial fretting wear depth and found that the relative displacement is easier to cause crack initiation compared to contact load. Furthermore, considering the effects of the contact condition and lateral loading behaviour on the local stress distribution and lifetime performance, Yu et al. [34] developed a serial 3D FE model of a seven-wire stand to discover the interface mechanism under longitudinal and lateral loading. They found that lateral loading can lead to uneven stress distribution and micro slip mainly occurred between helical wires. Kastratović et al. [35] created the suitable finite element model of the wire rope and investigated its mechanical behaviour with special emphasis on different types of contacts and different types of axial loadings, which provide a better understanding and prediction of the mechanical response for the sling wire ropes. Prawoto et al. [36] performed a study on the failure mechanism of wire rope using both numerical and experimental approaches. Further, they found that the wire rope failure models involved shearing in addition to regular necking. However, from the literature mentioned above, previous efforts focus mainly on the wear characteristics of rope wires, failure behaviour of the service wire rope and the finite element analysis for

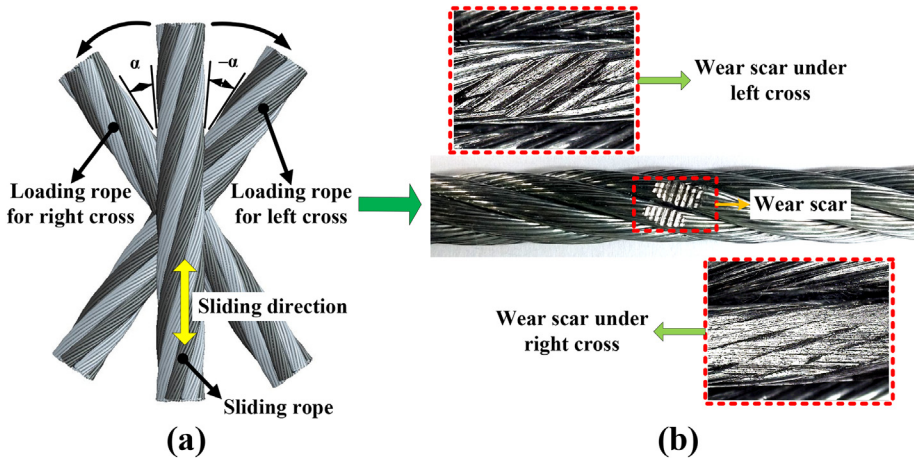


Fig. 1. Test rope sample (a): cross contact conditions for wear test; (b): wear scars on the rope surface.

the characteristics of the non-destructive wire rope and stands. The breaking failure features of wear-out wire ropes and the effect of different wear scars on the mechanical properties of the winding hoist wire rope have not previously been reported.

Therefore, the aim of this study is to investigate the fracture failure behaviour of the wear-out wire rope subjected to axial load and explore the application of the finite element analysis to the rope stand with different wear scars. Additionally, to obtain the rope samples for this research, the wear tests of the wire ropes under different cross contact conditions and the breaking tensile tests of the rope with surface wear have been carried out [2,8]. Then, the surface wear characteristics and cross section features of the broken wires were analyzed using the scanning electron microscopy (SEM). During the breaking tensile tests, the temperature variation in the wear scar region was monitored and collected using a thermal infrared imager to analyze the plastic damage of the wear-out wire ropes. Moreover, the 3D parametric models of the damaged rope stand were generated and imported into the Abaqus/CAE software. Further, the properties of the stress distribution of the strand with different wear scars were discussed. Additionally, this research is help for the understanding of the wear failure behaviour and will provide guidance for the safety use of the winding hoist wire rope. Then, the service life will be extended.

## 2. Experimental samples and study methods

### 2.1. Wire rope

The sample of this article is the wear-out  $6 \times 19 + FC$  (fibre core) point contact wire rope, as shown in Fig. 1b. In order to obtain the rope with different types of wear scars, the wear tests for the wire rope under different crossing angles and cross directions have been carried out. Fig. 1a presents the sliding contact conditions for the wear test. It can be seen that the wear tests were divided into two groups (left cross contact and right cross contact) and each test needs two wire ropes (sliding rope and loading rope). Therefore, different contact conditions will cause different wear scars for the loading ropes, particularly under the condition of different cross directions, taking into consideration the strand lay direction. Additionally, the diameter of the rope is 9.3 mm, the strand lay angle is  $15.5^\circ$  and other details of the wire rope can be found in the literature [2].

### 2.2. Methods

To explore the effects of the wear between wire ropes on the fracture failure behaviour, the breaking tensile tests were carried out for all the wear-out rope samples using a universal tensile testing machine (ZCGD-W1000KN). As shown in Fig. 2, it includes three major stages (elastic deformation, plastic deformation and fracture failure) in the process of breaking tensile. Thus, the thermal infrared imager was used to analyze the temperature rise characteristics during the plastic deformation. Additionally, the variation of the maximum temperature rise in the wear regions was quantitatively analyzed and compared between different test results. Then, the break location of the strands and the features of the surrounding wires were observed and discussed by the optical microscope and the SEM. Moreover, the finite element model was used to predict the mechanical properties of the rope strand with different wear profiles. As shown in Fig. 3, in order to make the geometrical model closer to the rope samples, the confocal three-dimensional contour measuring instrument (SM-1000) was used to measure the real value of the wear scars. Further, the wear contour can be obtained through the post-processing software (Mountains Map). Therefore, the parametric model of the damaged strand can be generated using the Pro/EngineerWildfire 5.0 and imported into the Abaqus/CAE software to analyze the stress distribution of the wear-out strands.

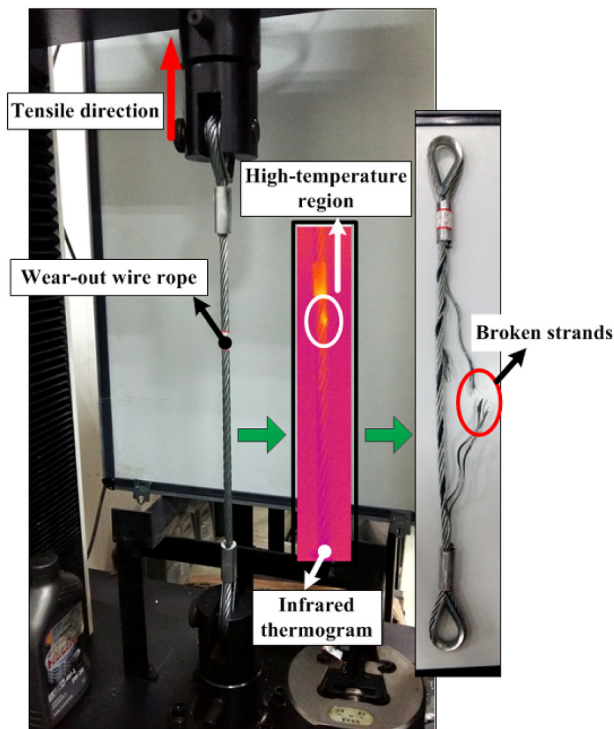


Fig. 2. Breaking tensile test of the rope.

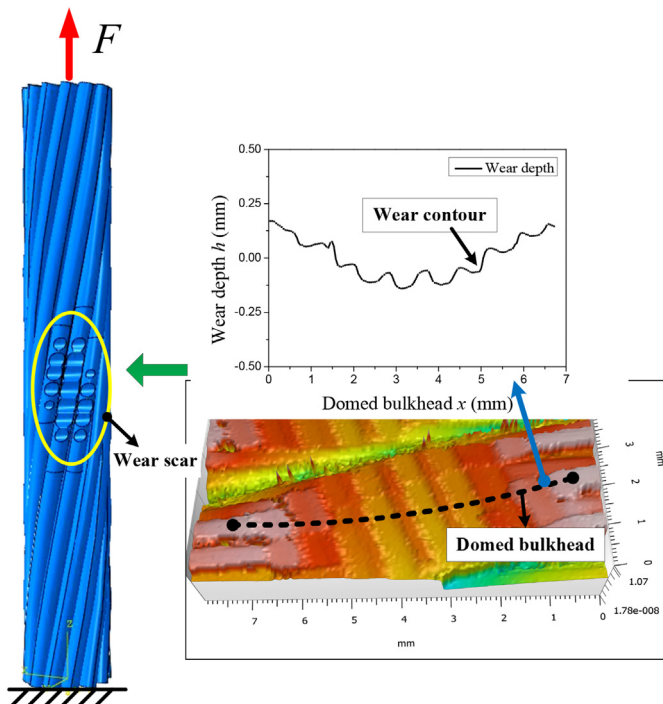


Fig. 3. Finite element model of the damaged rope strand.

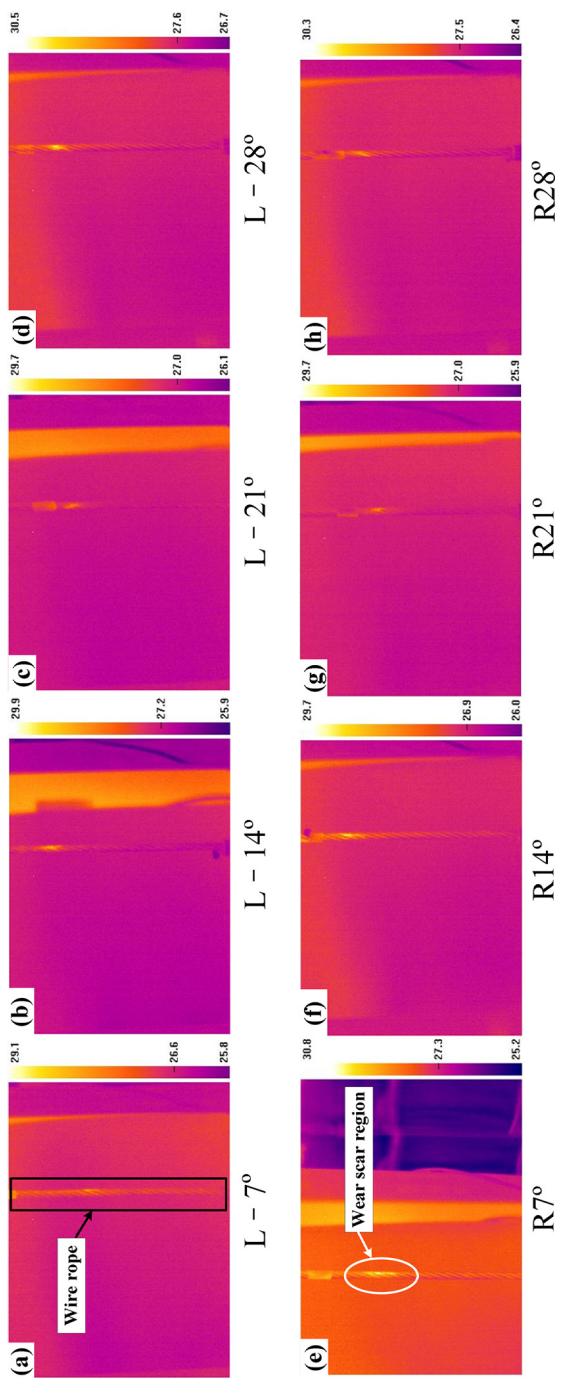
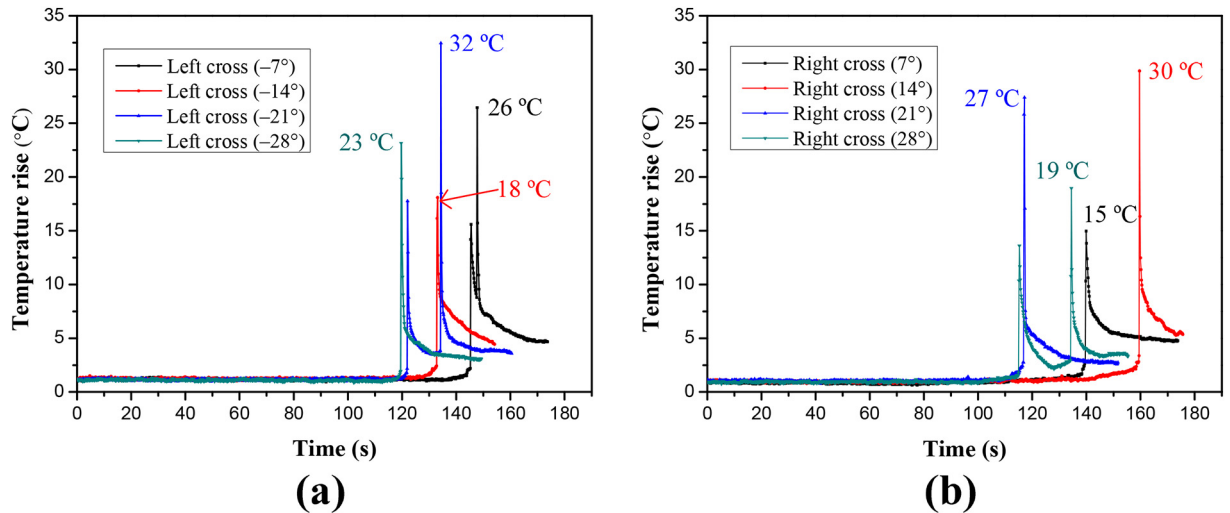


Fig. 4. Infrared thermograms of the rope samples with the wear scar caused by small crossing angle (a)–(d); left cross contact; (e)–(h); right cross contact.



**Fig. 5.** The temperature rise curves for the wear scar region under small crossing angle (a): left cross contact; (b): right cross contact (room temperature: 24 °C).

### 3. Breaking failure analysis

#### 3.1. The evolution of temperature rise during the breaking tensile tests

Fig. 4 shows the infrared thermograms of the wear-out wire rope samples obtained during the breaking tensile test. The bright area is the high temperature region in the images. As the plastic deformation of the materials will cause the temperature rise, the properties of the plastic phase for the rope samples can be analyzed through the change of temperature, which can determine the time and the location of the plastic deformation. Additionally, the wear tests were carried out for the wire rope under different crossing angles and cross directions. Thus, the rope samples with different wear scars can be divided into left cross contact (small crossing angle: from  $-7^\circ$  to  $-28^\circ$ ; larger crossing angle: from  $-50^\circ$  to  $-80^\circ$ ) and right cross contact (small crossing angle: from  $7^\circ$  to  $28^\circ$ ; larger crossing angle: from  $50^\circ$  to  $80^\circ$ ). Furthermore, there is a brighter area in the wire rope for all the tests. It indicates that the severe plastic deformation occurs in the wear scar region and the distribution of the wear will affect the characteristics of the deformation. As shown in Fig. 4e, when the crossing angle is small, the high temperature region in the rope sample is longer because the distribution of the wear region is larger and relatively even. Moreover, the plastic deformation is always accompanied by stress concentration. Therefore, through the monitor of the temperature variation, the analysis of the stress distribution for the rope samples was visualized.

To quantitatively analyze the temperature variation of the wire rope during the whole breaking tensile test, the maximum temperature rise in the wear scar region was calculated and the curves were obtained. Fig. 5 presents the temperature rise curves for the wear scar caused by small crossing angle. It is clear that the temperature is almost unchanged before approximately 120 s. Then it goes up to a maximum suddenly between approximately 120 s and approximately 160 s for each curve. Additionally, the characteristics of the curves are corresponding to different deformation stages of the rope samples during the breaking tensile test. In the beginning, the rope subjected to mechanical deformation and elastic deformation. Thus, the temperature remains constant. However, as the experiment continues, the plastic deformation begins to occur in the wear scar region, which causes the temperature increases rapidly. Due to the time of the plastic deformation before breaking is very short, the high temperature did not last long and decreased quickly, which correspond to the breaking stage. Furthermore, as the distribution of the wear scars is different, there are still many different characteristics of each curve. As shown in Fig. 5a, the time to reach the maximum temperature rise of each curve is different. When the crossing angle is  $-7^\circ$ , it is approximately 150 s to reach the maximum value. And it is approximately 120 s when the crossing angle is  $-28^\circ$ . It means the elongation of rope sample with wear scar caused by small crossing angle is larger and it needs more time to generate plastic deformation. Additionally, there are two peaks on the curve when the crossing angle is  $-21^\circ$ . It indicates the two wear-out strands did not break simultaneously. Moreover, the differences of the temperature rise curves are more obvious and are easier to distinguish, because the difference of the wear scar was more obvious under this sliding contact condition [8]. Furthermore, the stands in the rope sample with the wear scar caused by small crossing angle usually break simultaneously.

Fig. 6 presents the infrared thermograms of the rope samples with the wear scar caused by large crossing angle. The high temperature region in each rope is smaller compared with that in Fig. 4. Because the wear region is more concentrated in the condition of large crossing angle and the plastic deformation always starts in the wear scar region. Additionally, the colour of the images is brighter under the condition of right cross contact than that for the left cross contact. It means the plastic deformation is more severe for the wear scar under right cross contact. Therefore, the differences of the temperature distribution are able to reflect some characteristics of the wear scar and different types of sliding wear will influence the failure process of the wire ropes.

The evolution of the temperature rise in the wear scar region under left cross contact was shown in Fig. 7. It is clear that more

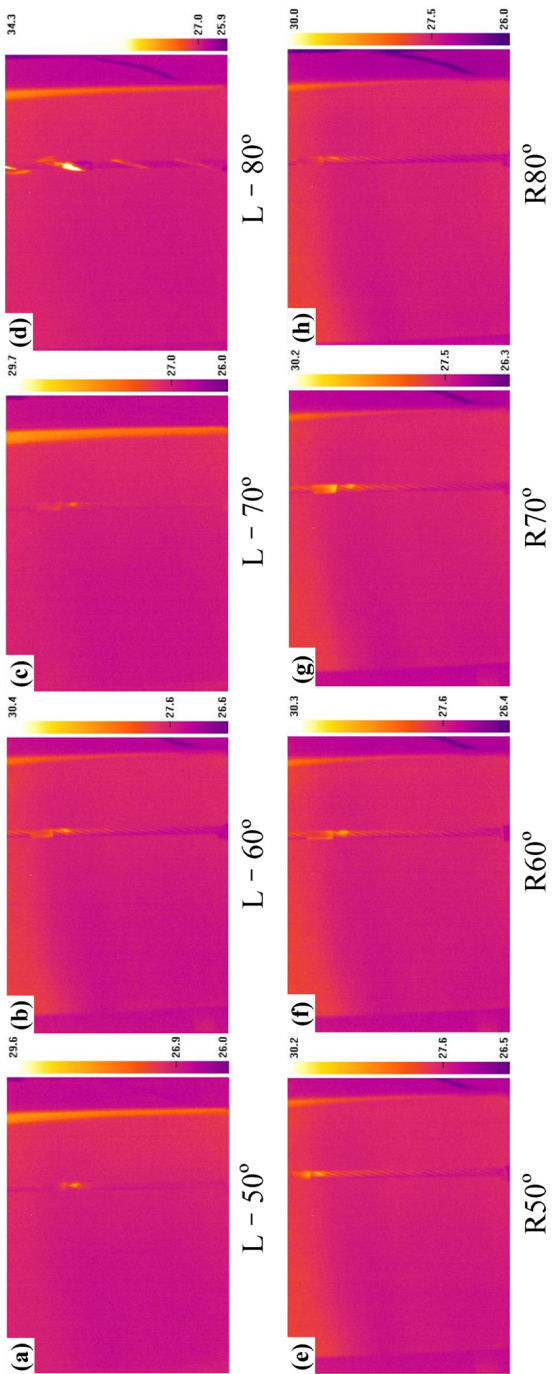
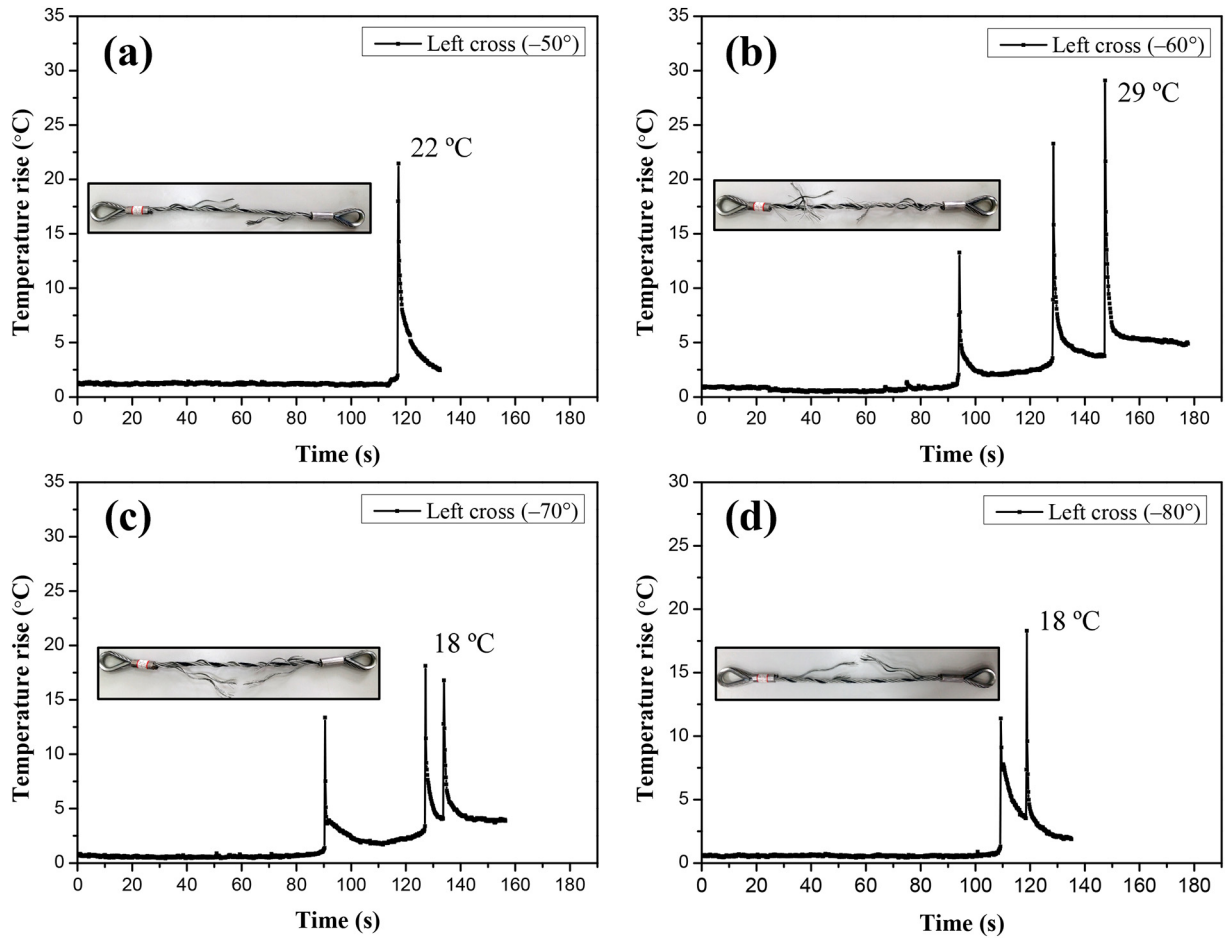


Fig. 6. Infrared thermograms of the rope samples with the wear scar caused by large crossing angle (a)-(d): left cross contact; (e)-(h): right cross contact.



**Fig. 7.** The evolution of temperature rise in the wear scar region under left cross contact.

peaks occur on the curves, in particular for Fig. 7b and c. There are three broken stands for the rope during the breaking tensile test. Additionally, each peck on the temperature rise curve represents one process of plastic deformation and fracture of the stands. When the sliding wear crossing angle is  $-50^\circ$ , there is only one peak on the curve, which occurs at the time of approximately 120 s. It indicates that the two damaged rope stands occur plastic deformation simultaneously before fracture. But, the three stands fracture at three different times (approximately 95 s, 130 s and 150 s) under the crossing angle of  $-60^\circ$ . This is because the distribution of the wear on strands is different under each crossing angle. In the case of small angle ( $-50^\circ$ ), the wear on the two strands is similar. Then, with the angle increases, the degree of wear on the two strands is different and the stress imbalance results in the strands fracture at different times. Furthermore, as the difference of the load carrying capacity between the strand subjected to mild wear and the strand without wear is not big, the tension did not less than the 50% of the maximum value for the test after the two wear-out strands fractured and there is one undamaged strand broken. Moreover, two peaks are very close (at approximately 125 s and 135 s) when the crossing angle increases to  $-70^\circ$  and it turns into two peaks for the curve at the crossing angle of  $-80^\circ$ . Because large crossing angle will cause large contact stress and lead to severe wear on the strands. Although the distribution of the wear on different strands is uneven, they are still easier to break than the undamaged strands. Therefore, the characteristics of the wear distribution caused by large crossing angle under left cross contact have a great influence on the fracture order of the strands in the wear-out wire rope.

Fig. 8 shows the temperature rise curves of the wear scar caused by large crossing angle under right cross contact. The maximum temperature rise for each curve is higher than that in Fig. 7 and the maximum value is approximately 38 °C as shown in Fig. 8b. Additionally, there are two peaks on the curve at most, which indicates that only two strands fractured during each breaking tensile test. When the crossing angle is  $50^\circ$ , the two peaks occur at approximately 140 s and 155 s, respectively. It means the rope sample subjected to larger elastic deformation before fracture. Furthermore, the distribution of the wear scar is more even in the case of  $60^\circ$  and  $70^\circ$  under right cross contact. Thus, the plastic deformation of the wear-out wire rope is primarily related to the distribution of the wear scar on different strands. The degree of wear determines the location of the fracture, which also provides reference for the non-destructive examination of the wire rope.

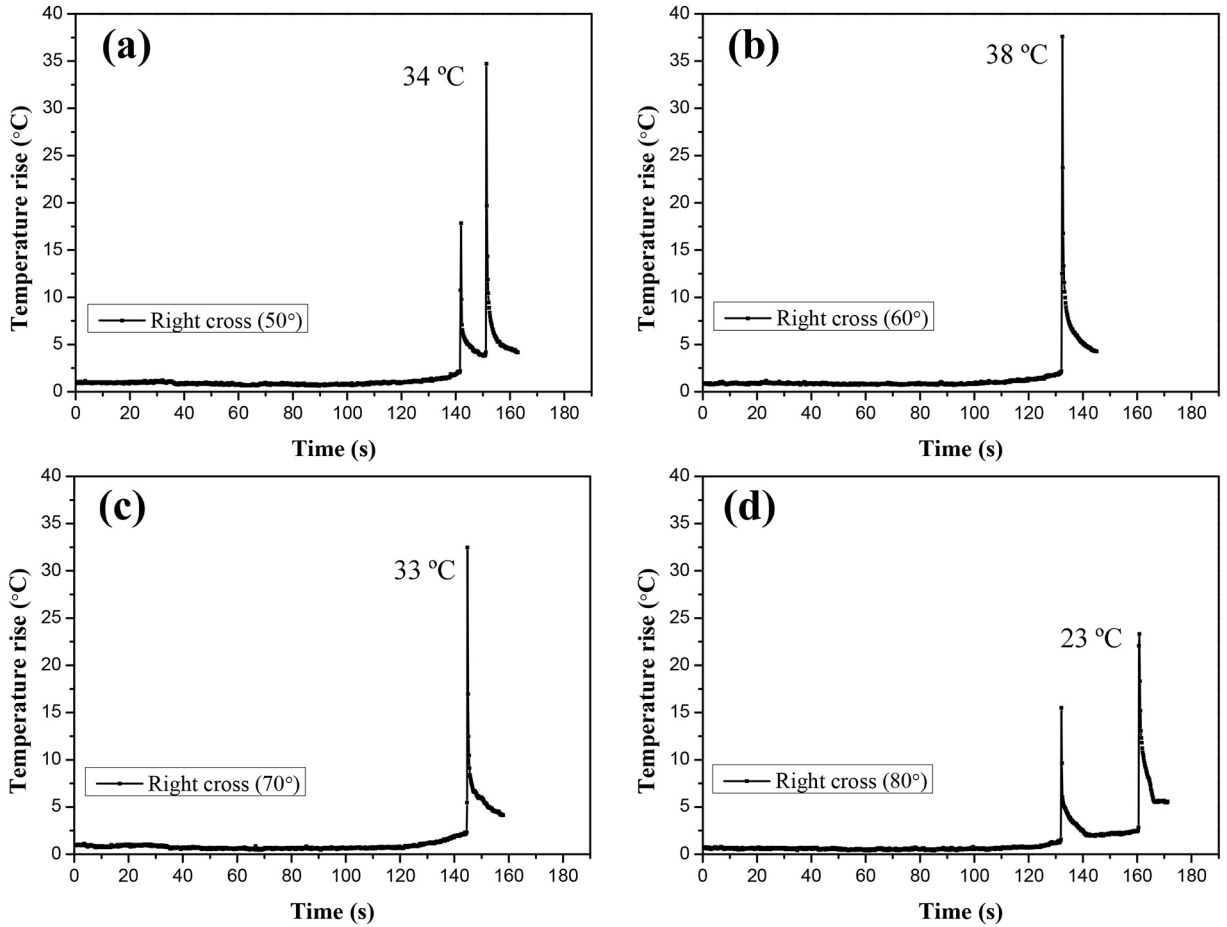


**Fig. 8.** The evolution of temperature rise in the wear scar region under right cross contact.

### 3.2. Fracture failure characteristics of the damaged wire rope

To analyze the failure characteristics of the rope samples under tensile load, the pictures of the fracture location in the strands were obtained using an optical microscope. Fig. 9 presents the optical micrographs of the fractured wires in the damaged strands. It can be seen that the wires can be divided into undamaged wires and wear-out wires. As shown in Fig. 9a, there is obvious necking phenomenon for the wire without wear scar. However, due to the wear distributes on the surfaces of outer wires, they fracture first with different wear scars. Furthermore, there is no obvious deformation at one end of the fracture for the damaged wires. It indicates that the stress concentration of wires is more obvious and the breaking process is faster than that for the undamaged wires. Additionally, different crossing angles for the wear test will cause different wear surface profiles, as shown in Fig. 9h and i. As the wear scar on the rope strands is consisting of the wear surface on the wires, the wear condition of the wires is different. The wear surfaces on many wires are similar to a plane, but the most surfaces of the wires are irregularity, which are consisting of many grooves. Moreover, the damaged wires always fracture at the place where the wear is most severe, as shown in Fig. 9b and e. The edge of the fracture surface usually distributes along the sliding wear direction. It also can be seen that the wires with larger wear depth are easier to fracture.

Fig. 10 presents the optical micrographs of the broken strands in the rope samples. Due to the wear distributes on the outer wires, the wear-out wires fracture first, as shown in Fig. 10a. The internal wires always fracture simultaneously at the location with the most fracture outer wires, and the broken internal wires still contact with each, as shown in Fig. 10c and d. It indicates that the stress state of undamaged internal wires is relatively more stable. However, the fracture of the outer wires is more scattered, which means the effect of the wear surface on the outer wires is more obvious under tensile load. It also can be seen that there is a certain distance between the fracture wear-out wires and the internal undamaged wires, which indicates the mechanical deformation and elastic deformation of the two kinds of wires are different. As shown in Fig. 10e, f and h, the internal wires' elongation is larger than that for the wires with wear scar. But, when the wear surface is more smooth and the wear region is larger (Fig. 10g and i), some wires will occur larger deformation and fracture later than that for internal wires. Therefore, the effect of the wear on the internal stress distribution of the strand is really obvious, in particular for the outer wires.

The wear characteristics of outer wires determine the fracture failure properties for the wire rope. Thus, the wear morphology on

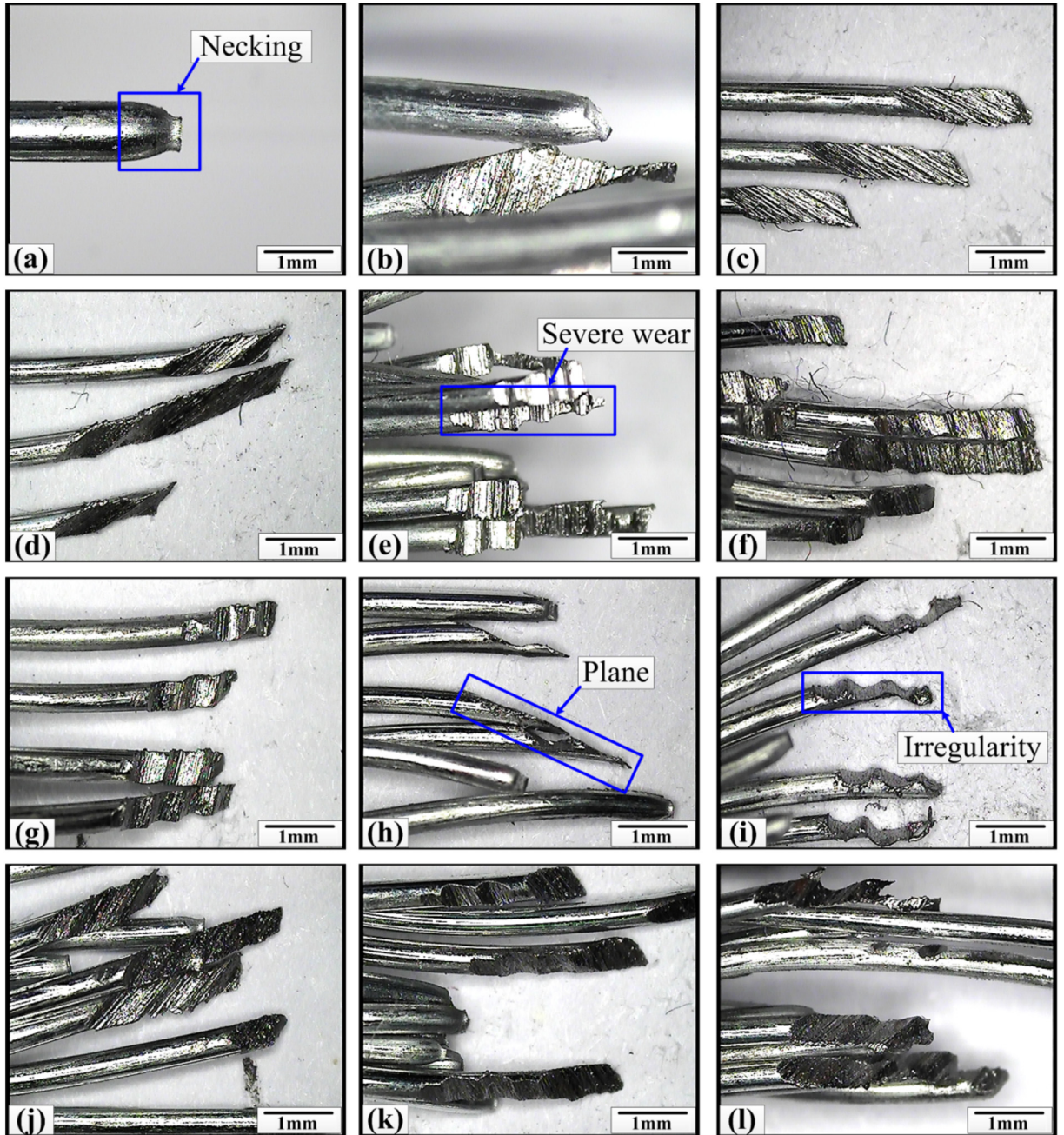


Fig. 9. Optical micrographs of the broken wires.

the broken wires was studied using the scanning electron microscope (SEM). Fig. 11 presents the SEM micrographs of the wear surface near the edge of the fracture for the wires. When the wear is mild on the wire surface (Fig. 11a and b), there is many debris on the edge of the wear region. The furrows are disorder and the wear depth is small. It indicates the contact pressure in the region is small and the fracture location has certain randomness. However, for the regions with severe wear, the surface is smoother and wear characteristics are directional. It is clear to seen the sliding wear direction (Fig. 11f). Furthermore, the plastic deformation and surface irregularities usually occur on the wear scar region, which will result in the uneven surface stress distribution and crack initiation, then ultimately lead to fracture of wires. This is the reason why the fracture happens first in the wear scar region of the wire rope samples. Moreover, the wear depth in the furrow is larger along the sliding wear direction. Thus, the wires always fracture along the furrows.

Fig. 12 shows the SEM micrographs of the fracture surface for the wear-out wires. It is clear that fracture section in the wear region is regular, which is similar to a line along the sliding wear direction. However, the other side of the fracture surface is

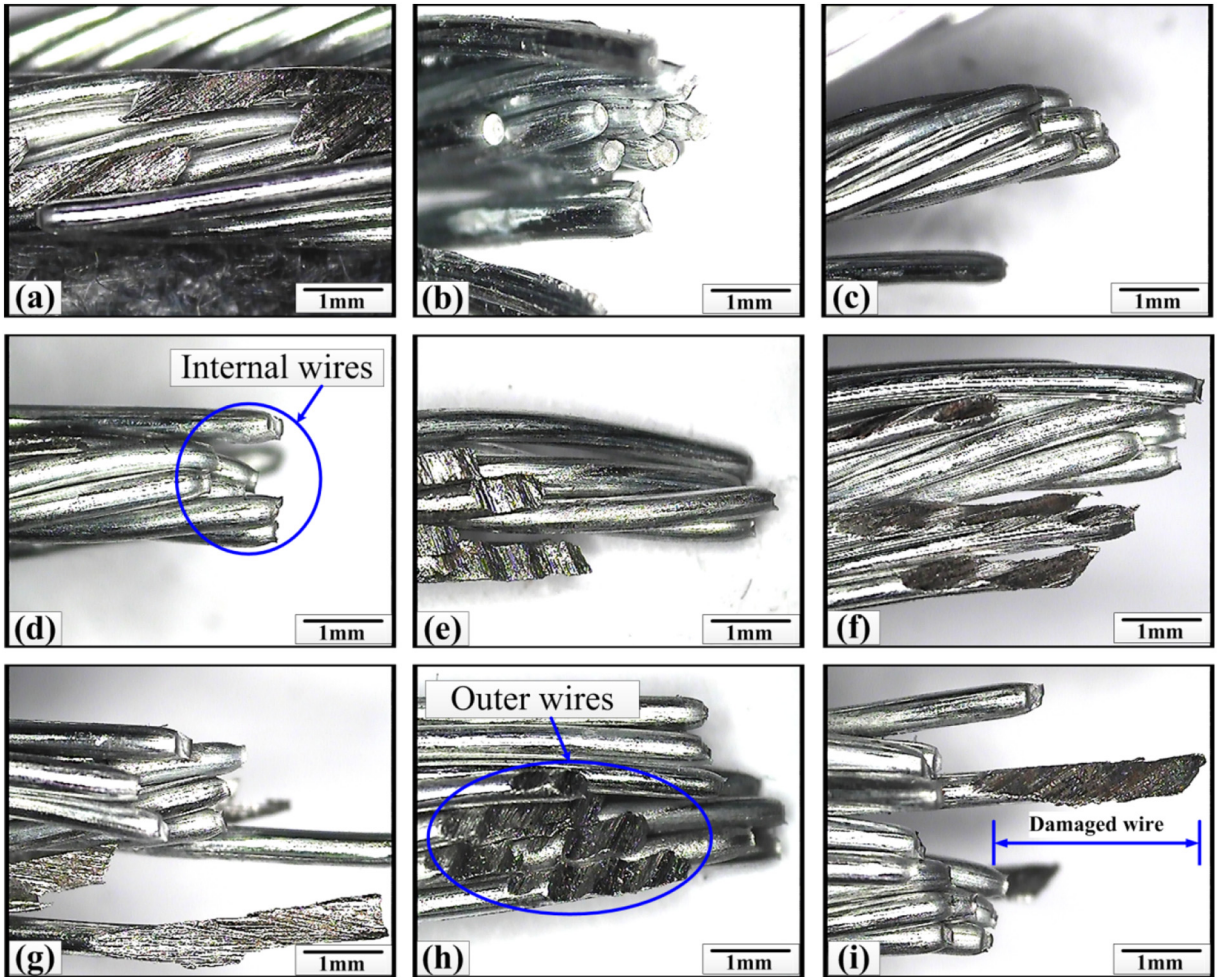


Fig. 10. Optical micrographs of the broken rope strands.

undamaged, there is slight plastic deformation and necking phenomenon. It indicates that the wear can reduce the plastic deformation before fracture of the wires. Therefore, the high temperature in the wear scar was caused by the severe plastic deformation of the undamaged internal wires. Furthermore, the failure mechanism of the wire rope is mainly ductile fracture.

#### 4. Finite element simulation

##### 4.1. Finite element model for the wear-out rope strands

The properties of plastic and fracture of the rope sample can be observed and analyzed visually, but the mechanical characteristics of the rope, in particular for the wear scar region are hard to be observed. Therefore, the finite element method (FEM) was used to study the effect of wear scars on the mechanical properties in the elastic stage. Due to the fracture first occur in the outer wires and the effect of the wear on the wear-out wires is more obvious, the simulation was carried out on the wear-out strands. Additionally, the wear has little effect on the fracture of the internal seven undamaged wires, they still contacted with each other in a spiral form after fracture, as shown in Fig. 10. Thus, the internal wires were treated as a whole in this model and this study was focused on the mechanical properties of the outer wires.

Fig. 13 shows the generation of the finite element model for the wear-out rope strand. Considering the complex helical structure of the wear-out outer wires, the geometric model of the important part of the strand was established by the Pro/EngineerWildfire 5.0. The core wire is easily generated using extrusion. The outer wires can be obtained by generating the centreline and using the variable section sweep along it. In the software, the four outer wires and core wire were generated. Then the similar wear scar shape was generated using the cutting extrusion, as shown in Fig. 13a. Taking into account different cross directions will cause different wear scar profiles, the strands with two typical wear surfaces, grooved surface and plane surface, were generated to analyze. Additionally, the undamaged strand and strand with wear scar caused by the crossing angle of 90° were also generated to realize comparative study. The centreline equation of the wires has been provided in references [29, 33]. Furthermore, the established models were

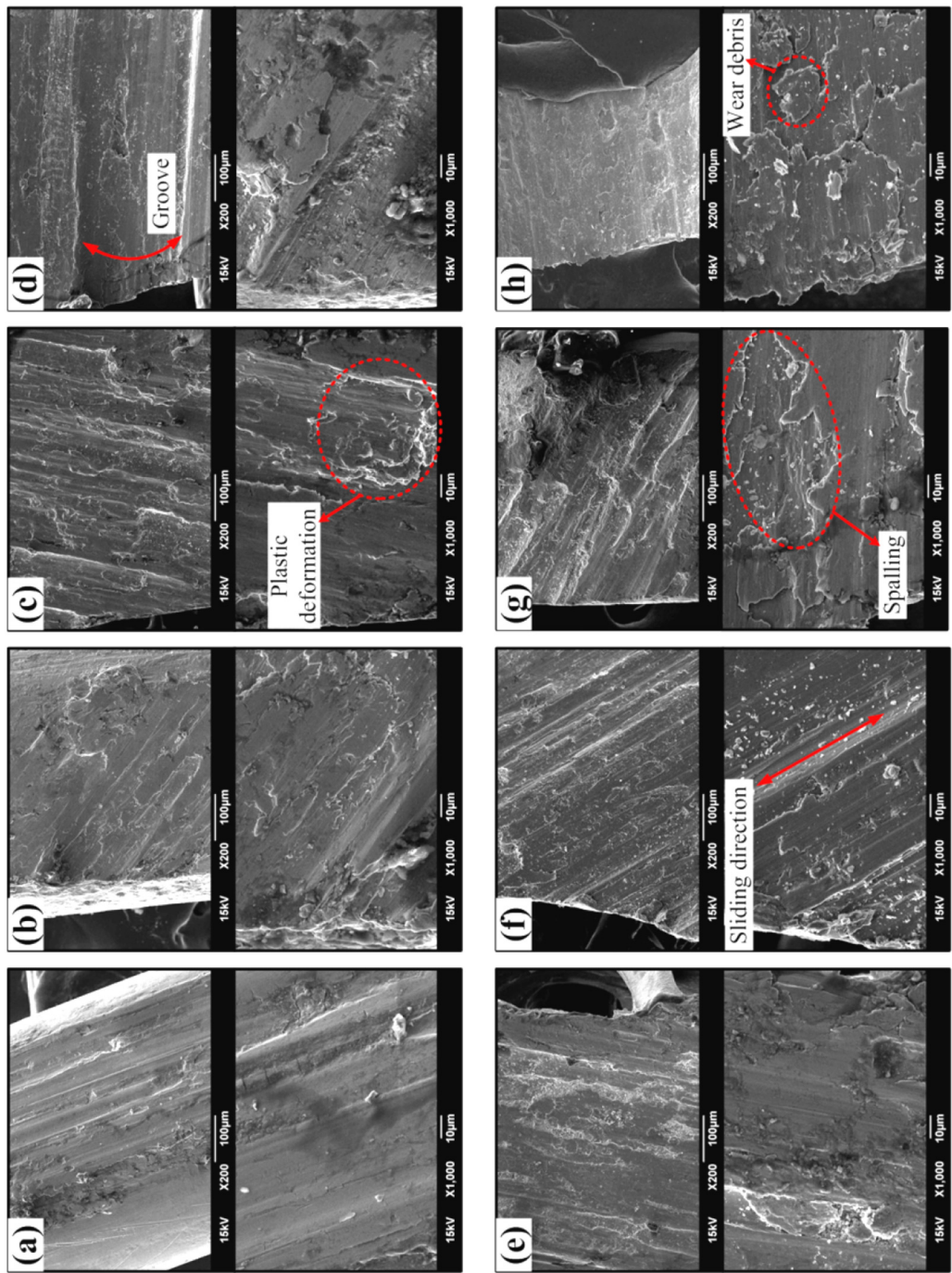


Fig. 11. SEM micrographs of the wear surface on the broken wires.

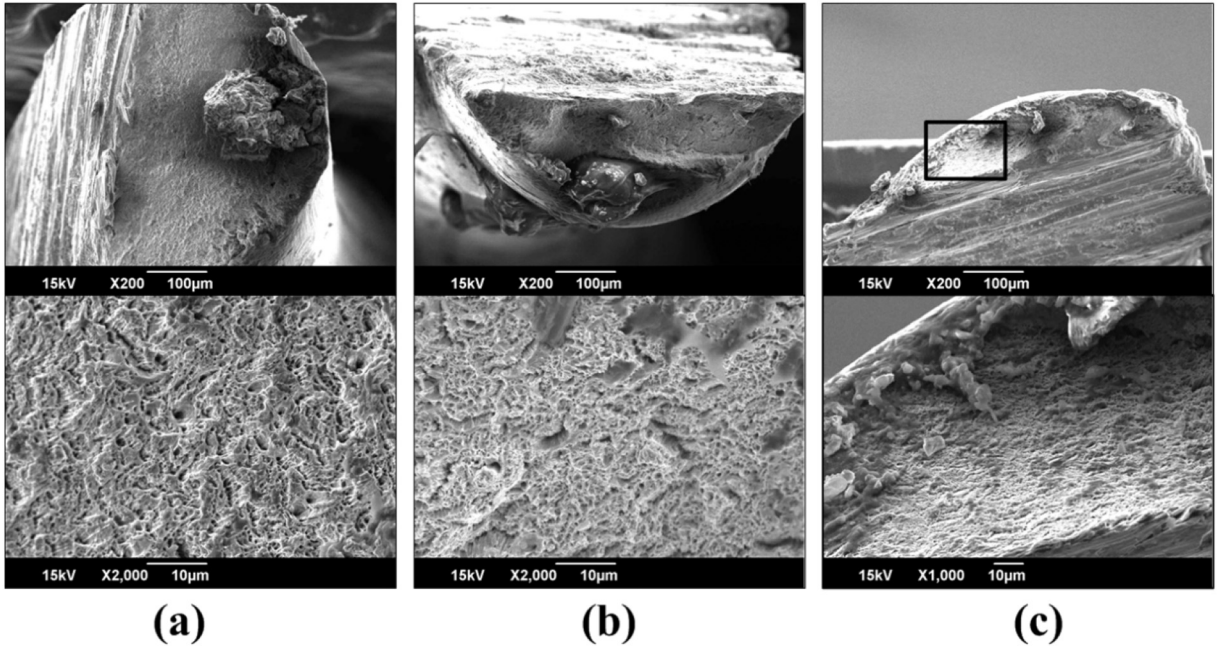


Fig. 12. SEM micrographs of the fracture surface for the wear-out wires.

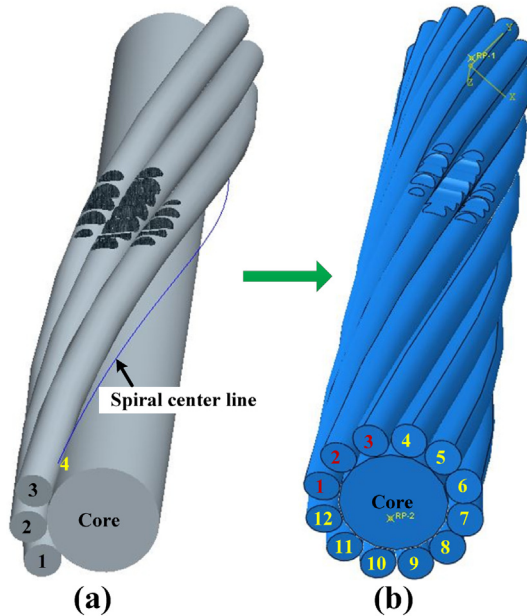


Fig. 13. Generation of the finite element model for the wear-out rope strand (a): Pro-E model; (b): FE model.

imported into the Abaqus/CAE. In the assembly module, the wire-4 was radially patterned along the strand axis to generate the wire-5 to wire-12. Then, the complete rope strand with wear scar was obtained. Moreover, the detailed geometrical and material parameters of the strand model are shown in Table 1.

The finite element method has been wildly used in the research of wire rope. Many scholars have created the finite element models for the wire rope to explore its mechanical properties [28–34]. The models' validity and reliability were validated by comparing the simulation results with the results of theoretical and experimental. Therefore, the similar method used for studying the characteristics of the wear-out wire rope subjected to tensile load is credible. Additionally, the commercial finite element analysis (ABAQUS) provides convenient parameter setting modules. In the interaction module, the surface-to-surface contact type was select to describe the contact behaviour between the adjacent outer wires and individual out wires and internal core wire under the condition of tensile load. The tangential behaviour and normal behaviour of the contact property were defined as penalty and hard

**Table 1**  
Geometrical and material parameters of the strand model.

Parameter	Value
Strand diameter	3 mm
Core wire diameter	1.8 mm
Helical wire diameter	0.6 mm
Wire lay length	40 mm
Strand lay angle	10.67 °
Model length	20 mm
Young's modulus	$1.95 \times 10^3$ MPa
Poisson's ratio	0.3
Density	$7.85 \times 10^3$ kg/m <sup>3</sup>

contact, respectively. The coefficient of friction between the contact surfaces was 0.2 [29,30]. Furthermore, two reference points (RP-1 and RP-2) were created to couple the cross section of the wires at each end, as shown in Fig. 14. Thus, it is convenient to add the axial tensile loading force (3000 N) and the completely fixed constraint at each end of the strand through this two reference points in the loading module. Considering the irregular structure of the wear region, the three wear-out wires in the strand were divided into three parts, respectively. Then, the eight-node linear brick element (C3D8R) with reduced integration and hourglass control was used for the undamaged parts of the strand, and the ten-node quadratic brick element (C3D10) was used for the wear region to realize the structural discretization. Moreover, the mesh size was controlled by the function of local seeds and the approximate size for the C3D8R and the C3D210 is 0.2 mm and 0.1 mm, respectively. Fig. 14 presents the whole model after mesh generation.

#### 4.2. Simulation results and discussion

Considering the differences of the wear scar profiles of the strand under different cross directions [2,8] and the need of comparative research, four finite element simulation models were created to explore the effect of typical wear scars on the mechanical properties of the outer wires in the strand. Fig. 15 presents the stress distribution of the wear-out and undamaged strands. As the simulation just studies the mechanical properties in the elastic stage, the maximum wear depth of the wear-out strands is 0.2 mm, 0.1 mm and 0.1 mm, respectively. It is clear that the stress of the outer wires under tensile load is symmetrically distributed and the effect of the wear scar is obvious. Additionally, there is obvious stress concentration and uneven stress distribution in the wear scar region compare with the result on the undamaged strand (Fig. 15d). However, the stress distribution characteristics are different in the different wear scar regions. When the crossing angle is 90° for the sliding wear test, the wear scar is consisting of many grooves. The stress concentration occurs at the bottom of the groove and the stress on both sides of the groove is much smaller, as shown in the stress nephogram (Fig. 15a). Furthermore, the wear scar under the condition of left cross is similar to that in the case of crossing angle at 90°, as shown in Fig. 15b. The maximum wear depth is smaller and the stress concentration phenomenon is not so obvious. But, the tendency of the stress distribution is similar. The stress is larger at the bottom of each groove and smaller on both sides of the groove. It indicates that the maximum wear depth plays an important role on the stress distribution of wear scar. Moreover, as the typical wear scar surface under the condition of right cross contact is a plane, as shown in Fig. 15c. The stress in the wear region is well distributed and there is no obvious stress concentration. Additionally, the stress in the wear scar region is still larger compared with that on the undamaged surfaces of the strand.

To quantitatively analyze and compare the difference of the stress distribution in the wear scars, the stress curves along the path in the wear region for the four simulation models were obtained, as shown in Fig. 16. The variation features of the stress curves are correspond to the wear scar profiles. When the crossing angle is 90°, the fluctuation of the curve is large and there are obvious peaks and valleys, which correspond to the stress distribution of the grooves in the wear scar. Additionally, when the wear scar was caused by left cross contact, the maximum wear depth is smaller. Although there are still fluctuations on the curve along the path, the stress is much smaller. Additionally, the variation of stress curves for the undamaged strand and the strand with wear scar caused by right cross contact are similar. The curves are smooth without fluctuation, but the values for the wear-out strand are larger. It means stress distribution of the two strands is relatively uniform and the stress concentration occurs on the wear-out strand. Therefore, when the wear scar is consisting of many grooves (left cross contact and cross contact at 90°), there is obvious stress concentration and uneven distribution in the wear scar region. The larger wear depth will cause much larger stress fluctuation. It is easier to result in the crack initiation of the wear-out wires at the maximum stress concentration. This is the reason why the wires fracture at the location with

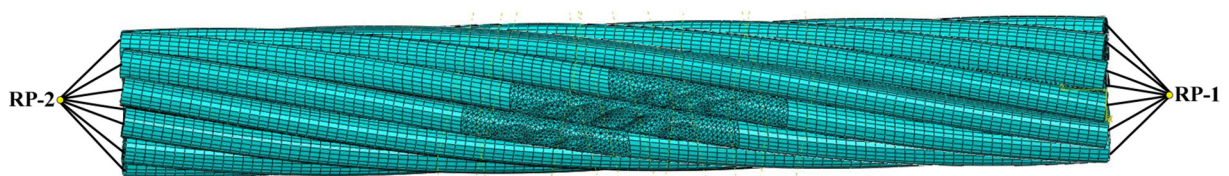
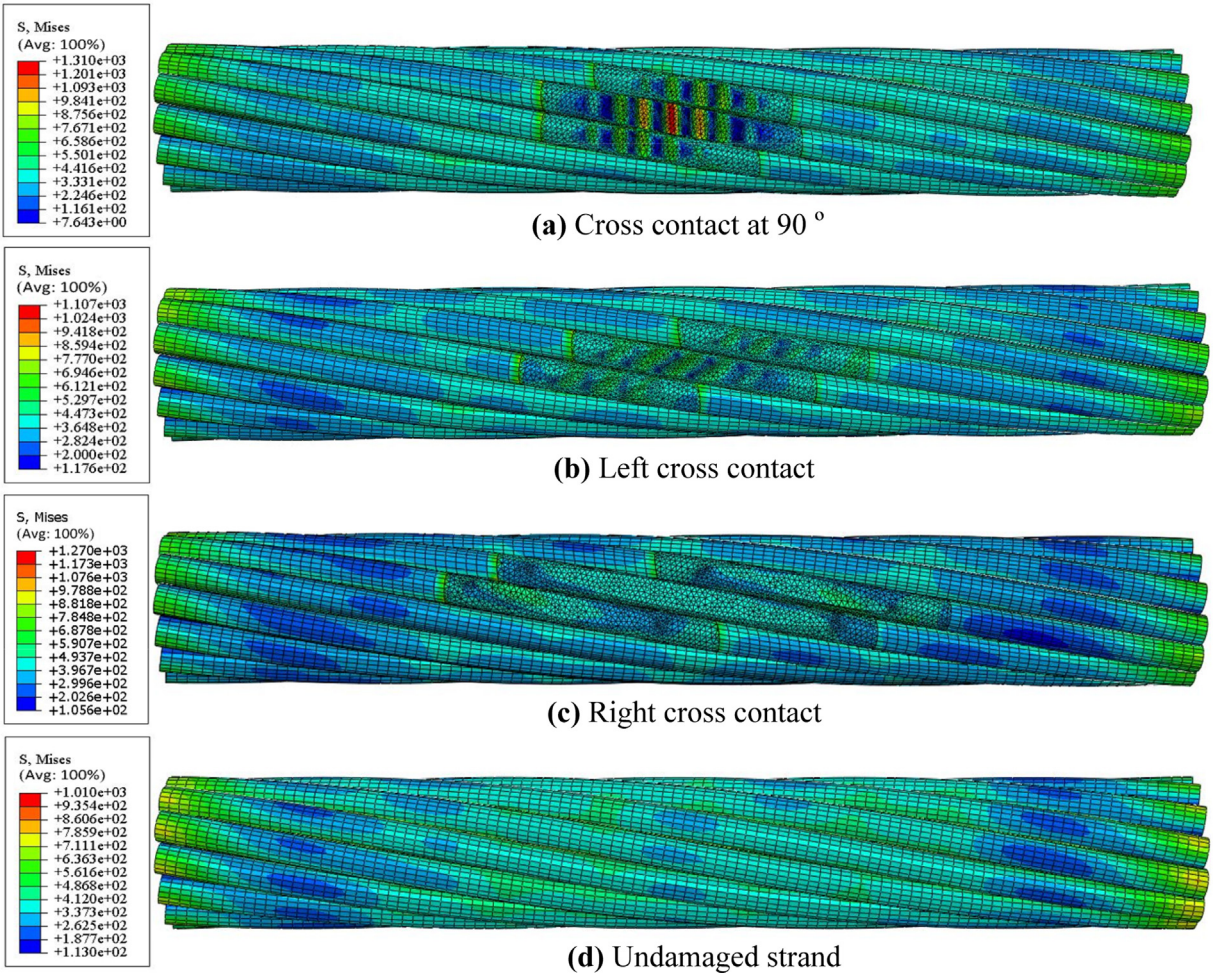
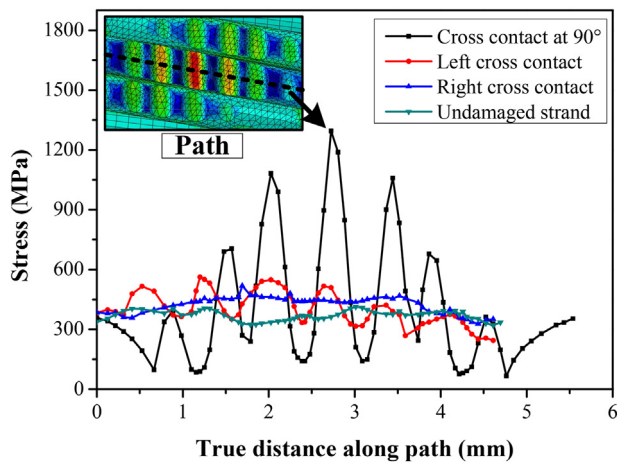


Fig. 14. The finite element model of the wear-out strand.



**Fig. 15.** Stress distribution (MPa) of the wear-out and undamaged rope strands at the tensile load of 3000 N.



**Fig. 16.** Stress curves along the path in the wear region.

the greatest wear depth, as mentioned in [Section 3.2](#). Additionally, the stress concentration of the wear scar under the condition of right cross contact will lead to the fracture of the wear-out wires, but the symmetrical stress distribution causes the randomness of the fracture location. Thus, the simulation results provide a good explanation for the fracture failure characteristics of the wear-out outer wires. The stress distribution is related to both of the wear depth and wear scar surface.

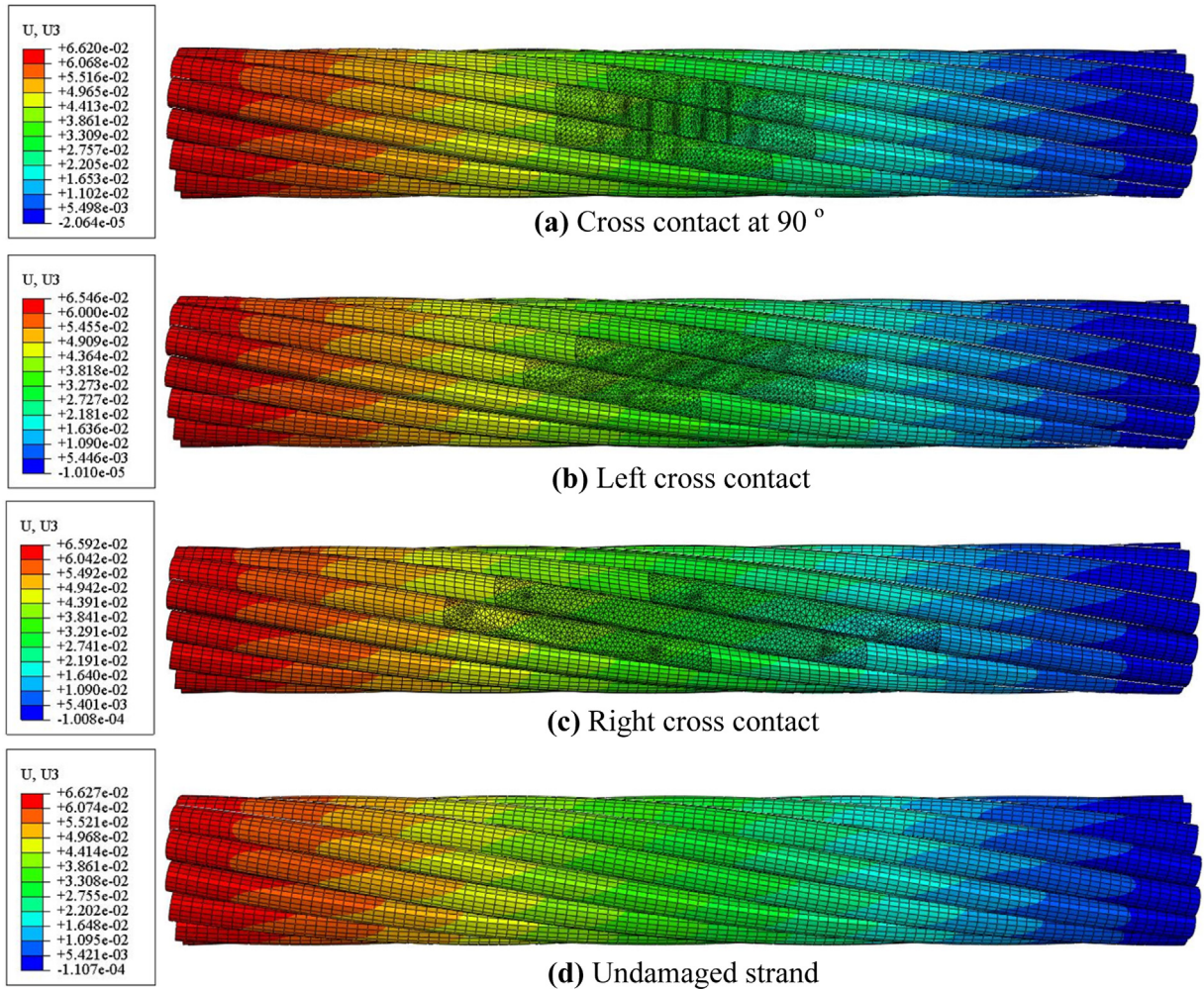


**Fig. 17.** Displacements (mm) of the wear-out and undamaged rope strands in the direction of Z coordinate axis.

Fig. 17 shows the displacements of the wear-out and undamaged rope strands in the direction of Z coordinate axis. Due to the one end of the finite element simulation models is fixed and the other free end subjected to the tensile load, the displacement of the free end is the largest and it decreases from the free end to the fixed end. It also can be seen that there is no obvious difference for the displacement distribution in the wear regions and on the surface of the undamaged strand. Thus, the effect of the surface wear on the axial elongation of the strand is small in the elastic stage by comparing the result of the undamaged strand, as shown in Fig. 17d. Additionally, the stress in the wear region is larger than the undamaged surface, but the larger stress did not cause large elongation in this regions. Therefore, the wear regions always start to fracture earlier than other place.

## 5. Conclusions

The present breaking failure analysis and finite element simulation of the wear-out winding hoist wire rope revealed the following findings:

1. The severe plastic deformation first occurred in the wear scar region of the wire rope and it will cause obvious temperature rise at the fracture location, approximately 20 °C to 30 °C.
2. The variation of temperature rise curves in the wear scar region can well reflect the number and the order of the breaking strands. The uneven wear distribution on the strand surfaces will reduce the degree of plastic deformation and increase the number of the fractured rope strands under the same breaking tensile test.
3. The wear-out outer wires always fracture earlier than the internal undamaged wires and the internal undamaged wires fracture simultaneously subjected to larger plastic deformation. Additionally, the fracture of the wires always occurs at the location with the maximum wear depth for the irregular wear scar and it usually fractures along the sliding wear direction.
4. The wear scar region will occur obvious stress concentration when the strand subjected to tensile load. There is obvious uneven

stress distribution in the irregular wear scar region and larger wear depth can make a significant contribution to this non-uniform distribution. Additionally, the wear has little effect on the elongation of the wear-out strand in the elastic deformation stage.

## Acknowledgements

This study is supported by The Fundamental Research Funds for the Central Universities (2018BSCXA15), Postgraduate Research & Practice Innovation Program of Jiangsu Province (KYCX18\_1954). The authors also wish to thank Top-notch Academic Programs Project of Jiangsu Higher Education Institutions (TAPP), and Project Funded by the Priority Academic Program Development of Jiangsu Higher Education Institutions (PAPD).

## References

- [1] V. Fontanari, M. Benedetti, B.D. Monelli, Elasto-plastic behavior of a Warrington-Seale rope: experimental analysis and finite element modeling, *Eng. Struct.* 82 (2015) 113–120.
- [2] X.D. Chang, Y.X. Peng, Z.C. Zhu, et al., Effects of strand lay direction and crossing angle on tribological behavior of winding hoist rope, *Materials* 10 (6) (2017) 630.
- [3] D.G. Wang, X. Li, X. Wang, Effects of hoisting parameters on dynamic contact characteristics between the rope and friction lining in a deep coal mine, *Tribol. Int.* 96 (2016) 31–42.
- [4] D.G. Wang, D.K. Zhang, S.R. Ge, Effect of terminal mass on fretting and fatigue parameters of a hoisting rope during a lifting cycle in coal mine, *Eng. Fail. Anal.* 36 (2014) 407–422.
- [5] C.R. Chaplin, The Fatigue and Degradation Mechanisms of Hoisting Ropes, Hoist and Haul Conference Perth, WA, 2005, pp. 5–7.
- [6] R.P. Singh, M. Mallik, M.K. Verma, Studies on failure behaviour of wire rope used in underground coal mines, *Eng. Fail. Anal.* 70 (2016) 290–304.
- [7] G. Rebel, R. Verreet, B. Schmitz, Degradation mechanism of wire ropes operating on multi-layer crane and mine hoisting drums, OIPEEC Conference Texas, 2011.
- [8] X.D. Chang, Y.X. Peng, Z.C. Zhu, et al., Experimental investigation of mechanical response and fracture failure behavior of wire rope with different given surface wear, *Tribol. Int.* 119 (2018) 208–221.
- [9] Ministry of Coal Industry, The Coal Mine Safety Rules, Coal Industry Publishing House, Beijing, 1986.
- [10] D.K. Zhang, S.R. Ge, Y.H. Qiang, Research on the fatigue and fracture behavior due to the fretting wear of steel wire in hoisting rope, *Wear* 255 (2003) 1233–1237.
- [11] D.G. Wang, D.K. Zhang, S.R. Ge, Effect of displacement amplitude on fretting fatigue behavior of hoisting ropewires in low cycle fatigue, *Tribol. Int.* 52 (2012) 178–189.
- [12] D.G. Wang, D.K. Zhang, W.J. Zhao, S.R. Ge, Quantitative analyses of fretting fatigue damages of mine rope wires in different corrosive media, *Mater. Sci. Eng. A* 596 (2014) 80–88.
- [13] A. Cruzado, M. Hartelt, R. Wäsche, M.A. Urchegui, X. Gómez, Fretting wear of thin steel wires part 1: influence of contact pressure, *Wear* 268 (2010) 1409–1416.
- [14] A. Cruzado, M. Hartelt, R. Wäsche, M.A. Urchegui, X. Gómez, Fretting wear of thin steel wires part 2: influence of crossing angle, *Wear* 273 (2011) 60–69.
- [15] A. Cruzado, M.A. Urchegui, X. Gómez, Finite element modeling and experimental validation of fretting wear scars in thin steel wires, *Wear* 289 (2012) 26–38.
- [16] A. Cruzado, M.A. Urchegui, X. Gómez, Finite element modeling of fretting wear scars in the thin steel wires: application in crossed cylinder arrangements, *Wear* 318 (2014) 98–105.
- [17] C.R. Chaplin, Failure mechanisms in wire ropes, *Eng. Fail. Anal.* 2 (1) (1995) 45–57.
- [18] K.M. Mahmoud, Fracture strength for a high strength steel bridge cable wire with a surface crack, *Theor. Appl. Fract. Mech.* 48 (2) (2007) 152–160.
- [19] P. Peterka, J. Krešák, S. Kropuch, et al., Failure analysis of hoisting steel wire rope, *Eng. Fail. Anal.* 45 (2014) 96–105.
- [20] G. Piskoty, M. Zgraggen, B. Weisse, et al., Structural failures of rope-based systems, *Eng. Fail. Anal.* 16 (2009) 1929–1939.
- [21] S. Karabay, A.T. Ertürk, M. Zeren, et al., Failure analysis of wire-breaks in aluminum conductor production and investigation of early failure reasons for transmission lines, *Eng. Fail. Anal.* 83 (2018) 47–56.
- [22] Y. Yu, Z. Chen, H. Liu, Advanced approaches to calculate recovery length and force redistribution in semi-parallel wire cables with broken wires, *Eng. Struct.* 131 (2017) 44–56.
- [23] M. Giglio, A. Manes, Life prediction of a wire rope subjected to axial and bending loads, *Eng. Fail. Anal.* 12 (4) (2005) 549–568.
- [24] R. Raišutis, R. Kažys, L. Mažeika, et al., Ultrasonic guided wave-based testing technique for inspection of multi-wire rope structures, *NDT & E Int.* 62 (2014) 40–49.
- [25] D. Zhao, S. Liu, Q. Xu, et al., Fatigue life prediction of wire rope based on stress field intensity method, *Eng. Fail. Anal.* 81 (2017) 1–9.
- [26] S. Lalonde, R. Guilbault, F. Légeron, Modeling multilayered wire strands, a strategy based on 3D finite element beam-to-beam contacts-part I: model formulation and validation, *Int. J. Mech. Sci.* 126 (2017) 281–296.
- [27] S. Lalonde, R. Guilbault, S. Langlois, Modeling multilayered wire strands, a strategy based on 3D finite element beam-to-beam contacts-Part II: application to wind-induced vibration and fatigue analysis of overhead conductors, *Int. J. Mech. Sci.* 126 (2017) 297–307.
- [28] E. Stanova, G. Fedorko, M. Fabian, S. Kmet, Computer modelling of wire strands and ropes. Part I: theory and computer implementation, *Adv. Eng. Softw.* 42 (2011) 305–315.
- [29] E. Stanova, G. Fedorko, M. Fabian, S. Kmet, Computer modelling of wire strands and ropes. Part II: finite element-based applications, *Adv. Eng. Softw.* 42 (2011) 322–331.
- [30] G. Fedorko, E. Stanova, V. Molnar, et al., Computer modelling and finite element analysis of spiral triangular strands, *Adv. Eng. Softw.* 73 (2014) 11–21.
- [31] E. Stanova, G. Fedorko, S. Kmet, et al., Finite element analysis of spiral strands with different shapes subjected to axial loads, *Adv. Eng. Softw.* 83 (2015) 45–58.
- [32] D. Wang, D. Zhang, S. Wang, et al., Finite element analysis of hoisting rope and fretting wear evolution and fatigue life estimation of steel wires, *Eng. Fail. Anal.* 27 (2013) 173–193.
- [33] D. Wang, D. Zhang, S. Ge, Finite element analysis of fretting fatigue behavior of steel wires and crack initiation characteristics, *Eng. Fail. Anal.* 28 (2013) 47–62.
- [34] Y. Yu, Z. Chen, H. Liu, et al., Finite element study of behavior and interface force conditions of seven-wire strand under axial and lateral loading, *Constr. Build. Mater.* 66 (2014) 10–18.
- [35] G. Kastratović, N. Vidanović, V. Bakić, et al., On finite element analysis of sling wire rope subjected to axial loading, *Ocean Eng.* 88 (2014) 480–487.
- [36] Y. Prawoto, R.B. Mazlan, Wire ropes: computational, mechanical, and metallurgical properties under tension loading, *Comput. Mater. Sci.* 56 (2012) 174–178.